ATLAS muon chamber construction at NIKHEF

NIKHEF ATLAS MUON GROUP
Contact: Marcel Vreeswijk, h73@nikhef.nl

November 2005

Abstract

At NIKHEF (Amsterdam), the largest muon chambers for the outer layer of the barrel ATLAS muon spectrometer have been constructed. At this facility, more than 40000 single drift tubes have been produced and 100 drift tube assemblies (muon chambers) have been constructed. We report on the quality assurance of both single drift tube production and chamber assembly. This, together with the also presented results from X-ray scans at CERN (Geneva) and results obtained in a dedicated cosmic ray test set-up, also part of the facility, demonstrates that the chambers fulfil ATLAS specifications.

Contents

1 Introduction **1**

2 Coordinate systems **3**

3 Drift tubes **4**

3.1 Drift tube requirements 5

3.2 Drift tube production 5

3.3 Drift tube quality 5

4 Drift tube chambers **10**

4.1 Assembly station 12

4.2 Chamber assembly 13

4.2.1 Results of X-ray scans 15

5 Chamber services **19**

6 Broken wires **21**

7 Tests of completed chambers **22**

7.1 Cosmic ray test stand 22

7.2 Results 22

8 Chamber transport to CERN and instalation in ATLAS **23**

9 Conclusions **24**

A Alignment system RASNIK **26**

List of Figures

1 *Picture taken in the fall of 2005 of the ATLAS detector under construction. The coils for the toroidal magnetic field can be recognized togheter with their support structures that also carries the muon system. On the bottom-right part of the picture, a drawing of a cross sectional view of the muon spectrometer is displayed, together with the feet that carry the ATLAS detector. This gives an impression of the location and size of the three layers of muon stations. The largest type of the outer layer, the BOL chamber is indicated. In the longitudinal direction (pointing in the paper) 12 muon chambers are positioned of each type. In the center of the picture, the calorimeter (not yet at its final position) is visible.* . . 1

2 *Illustration of the MDT measurment principle. The figure shows two muons entering a drift tube. One of the muons (the one in the back) passes relatively close to the wire and thus has small drift distance as indicated by the circle with corresponding radius. The other muon passes wire at a large distance as indicated.* 2

3 *Schematic view of a muon chamber.* 3

4 *Schematic view of a drift tube. Several components are indicated.* 4

5 *Picture of an end-plug and its components.* 4

6 *Picture of the wire machine taken at the south side. On the left the empty tubes come in. The tube in the center is being wired and will roll off at the right, where futher quality checkes are performed.* 6

7 *Scatterplot of the y and z deviation of the wire position measured on a sub-sample of produced drift tubes.* 7

8 *Leakrate of all used tubes in b l/s* 8

9 *a: Dark current in nA of all used tubes.* 8

10 *Measurement of the wire tension of all tubes just before chamber assembly.* 9

11 *Measurement of the change in wire tension between production of the tube and chamber assembly.* 9

12 *Schematic view of the sagadjustment system in the middle crossplate. Shown is the longbeam that is connected to this crossplate with a SPINDEL. By simply turning the SPINDEL the heigth of the middel cross plate with respect to the longbeam and is adjusted, enabling to align the middle crossplate with respect to the outer crossplates.* 10

13 *Schematic view of a chamber with several tubes left out to illustrate the stacking of tubes into layers.* 11

14 *finished BOL* 12

15 *Picture taken in the cleanroom showing the assembly table. Several key items are indicated.* 13

16 *a) The picture shows the stacking tower supporting the sphere in the extension of the spacer. The position of the extension is monitored by a RASNIK alignment system. b) This pictures shows the stacking tower together with the sag compensation tower.* 14

17 *Illustration of gastriplets.* 15

18 *Tube positions during assembly.* 16

19 *a) Glue dispension by the gluing machine. b) attaching another layer.* 17

20 *Illustration of the distribution of glue between the tubes in a multilayer.* 17

21 *Comparison of results from the tomograph scans for chambers BOL0, BOL2 and BOL3 with RASAS data taken during glueing of the layers of these chambers. For each chamber a set of 4 plots show the deviations from the nominal Z layer pitch for the 3 layers within each multilayer (MLI and MLII) at the HV and RO side respectively. xxxxxxxxxxxxxxxxxxkeep it? Then, renew itxxxxxxxxxxxxxxxxx* 18

22 *Picture of several alignment components.* 19

23 *Picture taken the HV side of a BOL chamber. Some individual tubes can be recognized together with the connections to the gasmanifolds. Also shown is a HV board and the backplate of the RASNIK mask component.* 20

24 *Picture taken at the RO side of a nearly completed BOL chamber. The RO electronics of the top and bottom multilayer is enclosed in Faraday cages. Also visible are the backplates of the RASNIK cameras, the DCS control box for the temperature and B field sensors, the readout motherboard and two RASMUXes as required for this specific chamber.* 21

25 *Picture of the cosmic ray stand with five BOL chambers. The chamber in the in the highest position is a small type BOL chamber with a width of 48 tubes.* 22

26 *Drift time distribution xxxxxxxxxxxxget xxxxxxxxxxxxxxxx* 23

27 *Residual. xxxxxxxxxxxxget plot if we want it.xxxxxxxxxxxxxxx* 23

28 *Efficiency for BOL002 as a function of the tube number.* 23

29 *Hit distribution for BOL002 as a function of the tube number.* 24

30 *Resolution for BOL002 as a function of the tube number.* 24

31 *The t_0 and t_{max} distributions for BOL002 as a function of the tube number.* 24

32 *Wire position deviation in the z direction for BOL002 as a function of the tube number.* . 25

33 *The principle of RASNIK.* 27

34 *Typical RASNIK image with the chess sboard pattern and the coded row and columns. The light intensity of the pixels under the indicated line is plotted, together with its derivative. The Gaussian peaks (positive and negative) determine the fine position of the image, as well as the image scale.* 28

1 Introduction

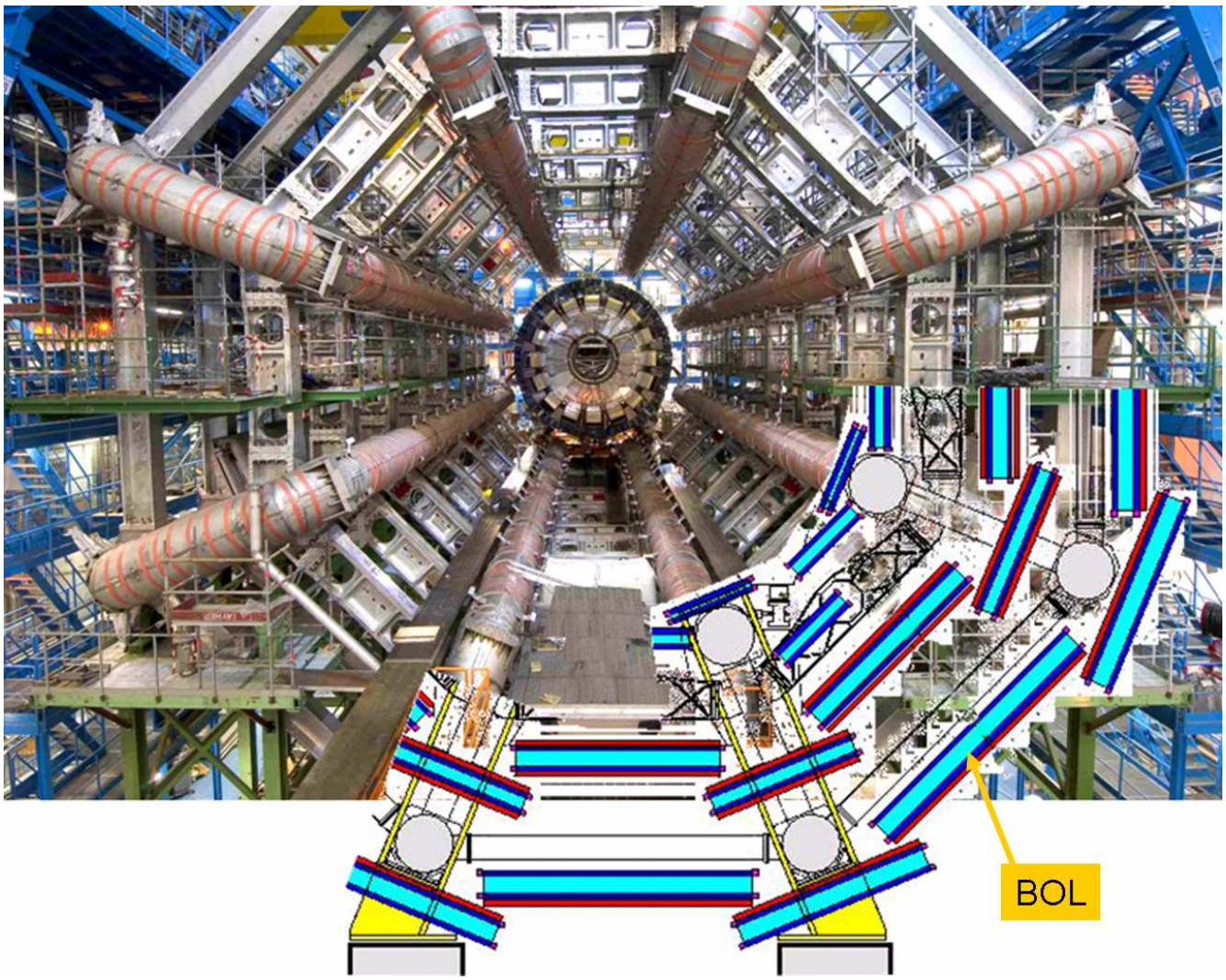

Figure 1: *Picture taken in the fall of 2005 of the ATLAS detector under construction. The coils for the toroidal magnetic field can be recognized togheter with their support structures that also carries the muon system. On the bottom-right part of the picture, a drawing of a cross sectional view of the muon spectrometer is displayed, together with the feet that carry the ATLAS detector. This gives an impression of the location and size of the three layers of muon stations. The largest type of the outer layer, the BOL chamber is indicated. In the longitudinal direction (pointing in the paper) 12 muon chambers are positioned of each type. In the center of the picture, the calorimeter (not yet at its final position) is visible.*

To stand-alone measure muons that emerge with a transverse momentum of 1 TeV/c with an accuracy $\frac{\sigma_{P_T}}{P_T}$=10% is the most stringent requirement for the muon spectrometer of the ATLAS experiment at the LHC. This translates to 50 μm uncertainty on the sagitta measurement in the 2 Tm integrated magnetic field, provided by an air core toroid.

The muon system in the barrel region ($\eta < 1$) is designed such that muon trajectories are measured by three muon chambers as illustrated in figure 1. All three layers consists of an approximately equal number of small and large type chambers. At NIKHEF (Amsterdam, The Netherlands) we constructed 100 'Barrel Outer Large' (BOL) chambers, including four spare chambers.

Muons chambers consist of accurately assembled layers of alumnium drift tubes. A drift tube has a diameter close to 3 cm and is closed by two end-plugs that hold a 50 μm thick tungsten wire. Under

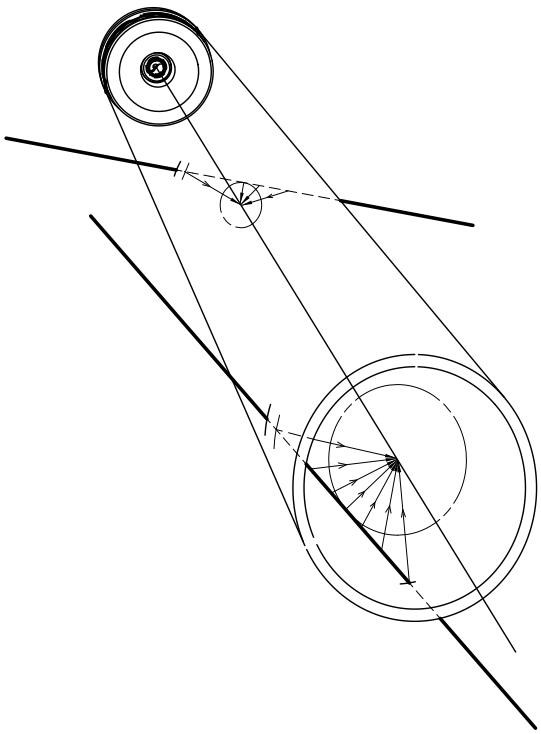

Figure 2: *Illustration of the MDT measurment principle. The figure shows two muons entering a drift tube. One of the muons (the one in the back) passes relatively close to the wire and thus has small drift distance as indicated by the circle with corresponding radius. The other muon passes wire at a large distance as indicated.*

operational conditions, the tube is filled with an Ar/CO_2 mixture of 93%/7% and the wire is set a potential of 3xxxxxx V with repect to the grounded tube wall. When a muon traverses the tube, it ionises the gas and the free electrons drift to the wire, generating a signal. The Read-Out electronics measure the arrival time of the signal above an adjustable threshold as shown in figure 2. The arrival time, containing the actual drift time information, is offline used to determine the drift radius based on a known relation between drift time and radius. Earlier tests show that the drift tubes under well-controlled conditions have single hit resolution of about 80 μm (averaged over drift distance), see [1]. The muon chambers in ATLAS have each at least 2×3 drift tube layers, providing sufficient drift radii to recognize and reconstruct a track segment with high accuracy.

The BOL muon chambers consists of two separate layers (multi-layers), each with three drift tube layers, mounted on an aluminium support structure (spacer) as shown in figure 3. Physical deformations of the chambers during construction, transport and operation are monitored [1] with an integrated, so called 'in-plane', alignment system also indicated in figure 3.

The combination of the uncertainties on single hit resolution, alignment and mechanical precision of the

[1] For this reason the ATLAS muon chamber are called Monitored Drift Tube (MDT) chambers

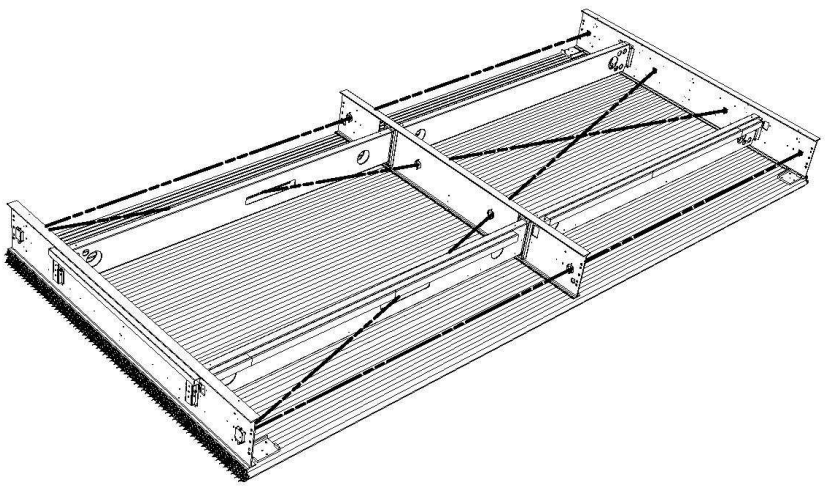

Figure 3: *Schematic view of a muon chamber.*

chambers should not exceed 50 μm to meet the aforementioned accuracy on the sagitta measurement. Simulations have indicated that is is required to construct the chambers with a mechanical precision of 20 μm (RMS), which is of unprecented accuracy for such large detectors.

In this report, we describe the production of single tubes and completed BOL chambers, moreover we present the results on the quality assurance operations. Among the tests is the dedicated measurement in the X-ray tomograph at CERN of a limited number (roughly 10%) of the BOL chambers. Finally, we summarise the muon chamber performance in the cosmic ray set-up at our facility.

2 Coordinate systems

For later use we define the coordinate systems. When the chamber is located on the assembly station in the 'upward' position the local chamber coordinates are defined such that the y coordinate points to the sky, the x coordinate runs along the tubes in the horizontal plane. The z coordinate, the precision coordinate, runs perpendicular to the tubes. The x, y and z axis constitute a left-handed coordinate system. The global coordinate system in our cleanroom is then defined by a south-north and west-east direction that runs in the x and z direction respectively. In the 'upward' position, the Read-out (RO) and High-Voltage (HV) side of the chamber coincides with the south and north respectively. In addition, for engineering purposes, we defined the west side of the setup as the 'reference-side'. The reference side always coincides with the smallest z coordinate of the chamber.

3 Drift tubes

A schematic view of a drift tube is shown in figure 4. A drift tube has a diameter of 29.970 ± 0.015 mm

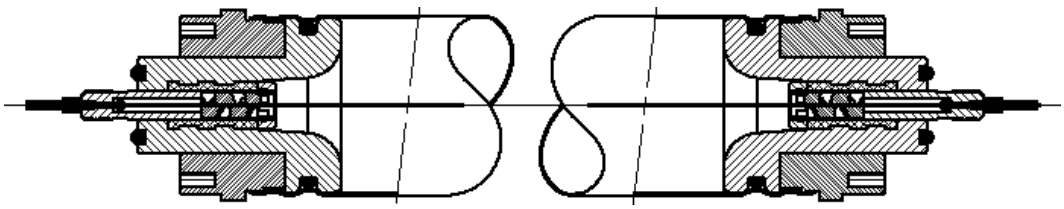

Figure 4: *Schematic view of a drift tube. Several components are indicated.*

and a wall thichness of 400 μm . The tube is swaged on two precise end-plugs that are manufactured with a precise outer ring of aluminium to position the tube during the assembly in jigs with high precision. The end-plug also connects to the gas system and is closed by a signal cap to connect High Voltage (HV) and Read-Out (RO) electronics boards at the tube's HV and RO ends respectively.

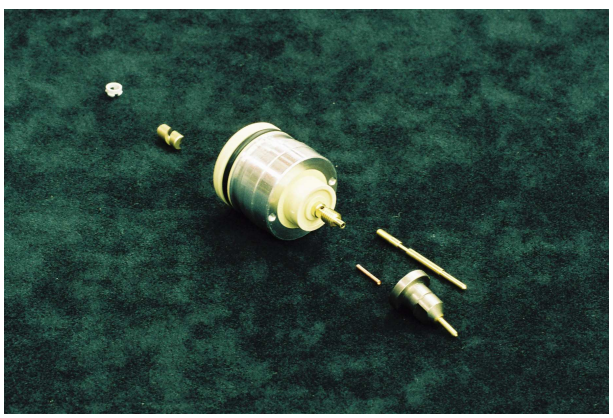

Figure 5: *Picture of an end-plug and its components.*

The 50 μm gold-plated tungsten wire is tensioned at 285 gram and then crimped into the end-plug. A locator ('twister') with small gas flow resistance, accurately centres the wire with respect to its outer ring.

3.1 Drift tube requirements

The meet the precision requirement on the total chamber, the contribution of individual drift tubes has to remain well below 20 μm to accomodate the finite accuray of the tube positioning during chamber assembly.

This imposes the accurate machining of the end-plugs and wire locators, which determine the position of the wire near the tube ends. We required the precision rings be machined within 10 μm with respect to the axis of the endplugs.

Near the middle of the tube, away from the endplugs, the wire tension determines the position of the wire (with respect to the precision ring). The wires of the BOL chambers are tensioned at 285 gram, which corresponds to a maximal gravitational sag of 406 μm . To limit the uncertainty (RMS) on this value to 10 μm precision an accuracy of 7 gram is required on the wire tension.

The requirement on the co-centricity of the wire due to non-straightness of the drift tube (anode-cathode distance) is a second order effect and set at 100 μm RMS.

Other than the mechanical precision we impose:

- the dark current of individual drift tubes shall not exceed 10nA at 3300V at 3bar absolute pressure with an Ar/CO_2 (93%/7%) gas mixture (gas gain 2×10^4),
- the leak rate under these conditions must be less than 10^{-8} bl/s.

These requirements ensure long term stable operation in the ATLAS experiment.

3.2 Drift tube production

The 40 thousand drift tubes were produced in the temperature-controlled cleanroom parallel to the assembly of the chambers, using a semi-automated wiring machine. On the picture shown in figure 6, taken at the south side (as we define it), several components are indicated.

The machine is loaded by an aluminium tube and two complete endplugs. The wire is transported from its supply by means of airflow through the 'south' end-plug toward the 'north' end of the tube. At the north end the wire is literally sucked through the end-plug and fetched by a wire clamp. Now, movable platforms at both sides bring the end-plugs to their final positions in the tube. The two end-plugs are fixed by tube swager using air pressure. At the south end, the wire is fixed at the left end-plug by crimping it and the tube is in the state as shown in the picture. The clamp at the other side moves away to pre-tension the wire by 400 gram before releasing it slowly to its final tension of 285 gram. Crimping the wire at the north end-plug finalises the drift-tube.

3.3 Drift tube quality

The wire tension, length and position was measured immediately after production for every tenth tube to assure proper operation of the wiring machine.

The tension is derived from the measurement of the fundamental harmonic resonance. This measurement is als used in [8] and it is based on the induced response to a sinusoidal current while the tube is partially immersed in a magnetic field.

The wire position with respect to the outer ring of the end-plug was measured using an eletromagnetic method (see [5]). the method uses the response of two coils sensing the field of an sinusoidal current that is driven through the wire. One set of coils is used at each end of the tube and by rotating the tube by 90 degrees two projections (called y and z) for each end are obtained.

Figure 7a shows a scatter plot of these projections. The radial deviation is better than 10 μm (RMS) as

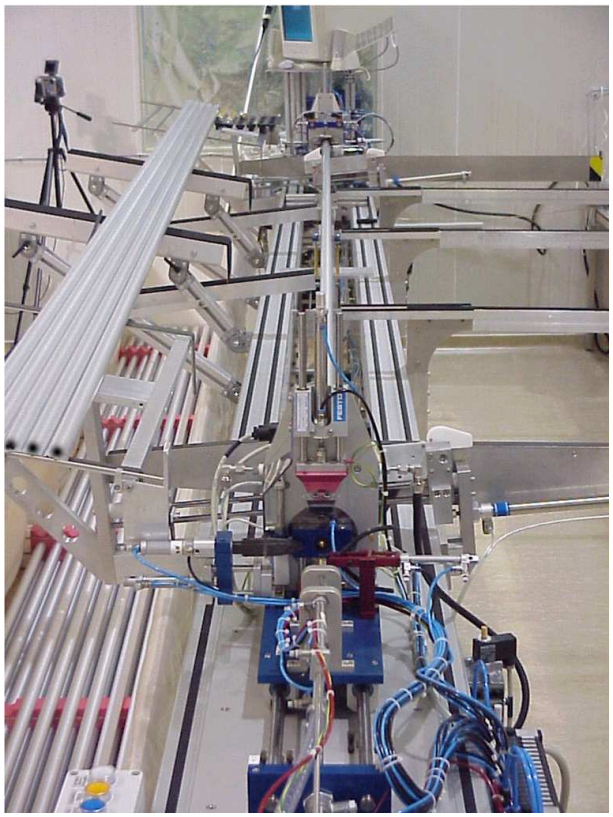

Figure 6: *Picture of the wire machine taken at the south side. On the left the empty tubes come in. The tube in the center is being wired and will roll off at the right, where futher quality checkes are performed.*

appropriate. In these tests, we found only eleven tubes with a deviation larger than 25 μm in one of these projections, which we stored for further (destructive) studies.

The gas tightness and dark current of all produced tubes was measured in a set-up (in the cleanroom) specially designed for this purpose. This set-up consists of 80 vacumized large tubes (diameter 6xxxx cm) loaded with the drift tubes under test. The drifttubes are filled with 4 bar 1%/99% helium/argon mixture and the wire is set at 3300 V. The leakrate (for Ar/CO_2 at 3 bar) and dark current measurement is shown in figure 8 and 9 respectively. The results indicate that the majority of the tubes is well within specifications. However, the long tail of the leakrate distribution (not shown) leads to a failure rate of about 1%, making the leakrate the dominant rejection source.

After ageing of at least one month and just prior to using the tubes in the actual chamber assembly, all the tubes were subjected to a second wire tension test. Like the frist measurement, the tension is also derived from the measured resonance frequency, but without the requirement that the tube is immersed in an magnetic field. The electrostatic force due to a supplied sinusoidal HV leads to mechanical wire oscillations. The changing capacity of the tube is measured in an LC circuit, leading to a resonance curve. the method is described in [4]. For our wire with length 4940 mm a weight per unit length of 38.70 mg/m, a resonance frequency of 27.2 Hz corresponds to 285 gram. The results of the second tension measurmeent are shown in figure 10. The precision of the wire tension over the full period of time is 0.33 Hz, which correcponds to about 6 gram (or 8 μm maximal sag). We decided to reject tubes with deviations larger than 1.5 Hz away from the nominal value, which led to the rejection of 21 tubes.

As mentioned above, for 10% of the tubes a 'fresh' measurement of the wire tension is available, allowing to study 'slippage' that may occur over time. We expect that if any slippage occurs, it occurs dominantly in the in the ageing period and possibly during handling of the tubes. // No evidence for wire slippage was found. The change in resonance frequency exhibits an assymetric shape as shown in figure 11. This suggest a comfortably small wire slippage for a fraction of the tubes.

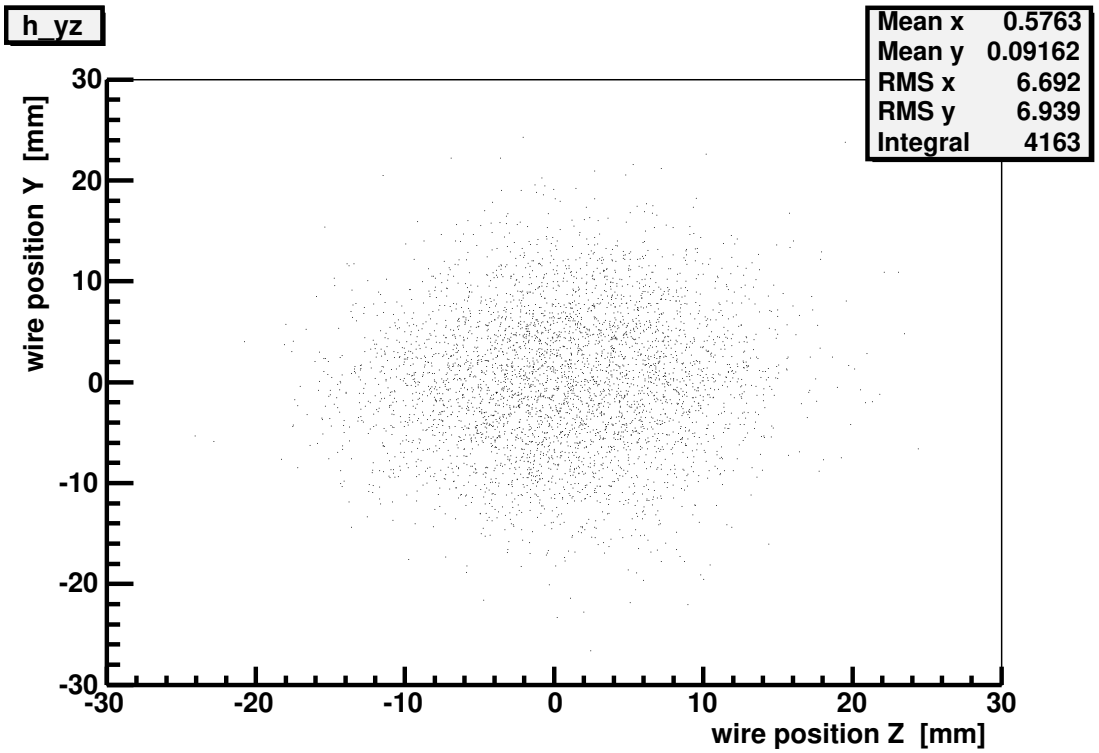

Figure 7: *Scatterplot of the y and z deviation of the wire position measured on a sub-sample of produced drift tubes.*

In total, we have produced about 40000 drift tubes. Our stringent criteria led to a rejection rate of 2.5%. The 100 BOL chambers (96 ATLAS chambers and 4 spares) we produced, contain 38448xxxxxxx tubes that fullfil our requirements.

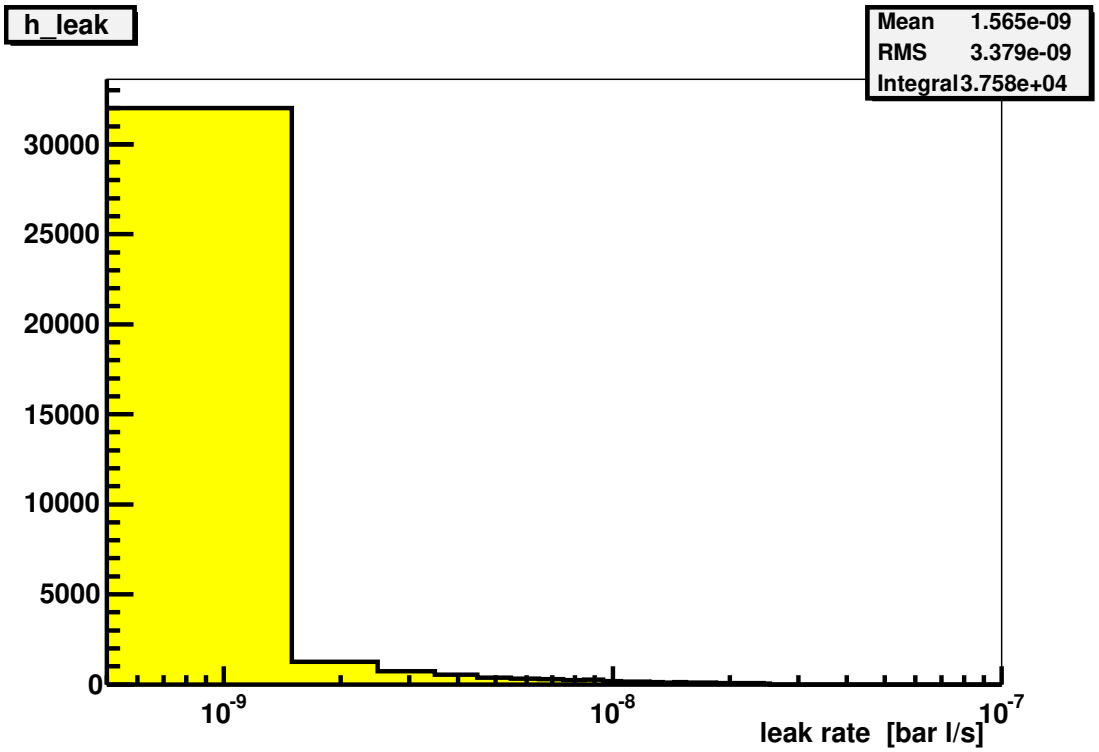

Figure 8: *Leakrate of all used tubes in b l/s*

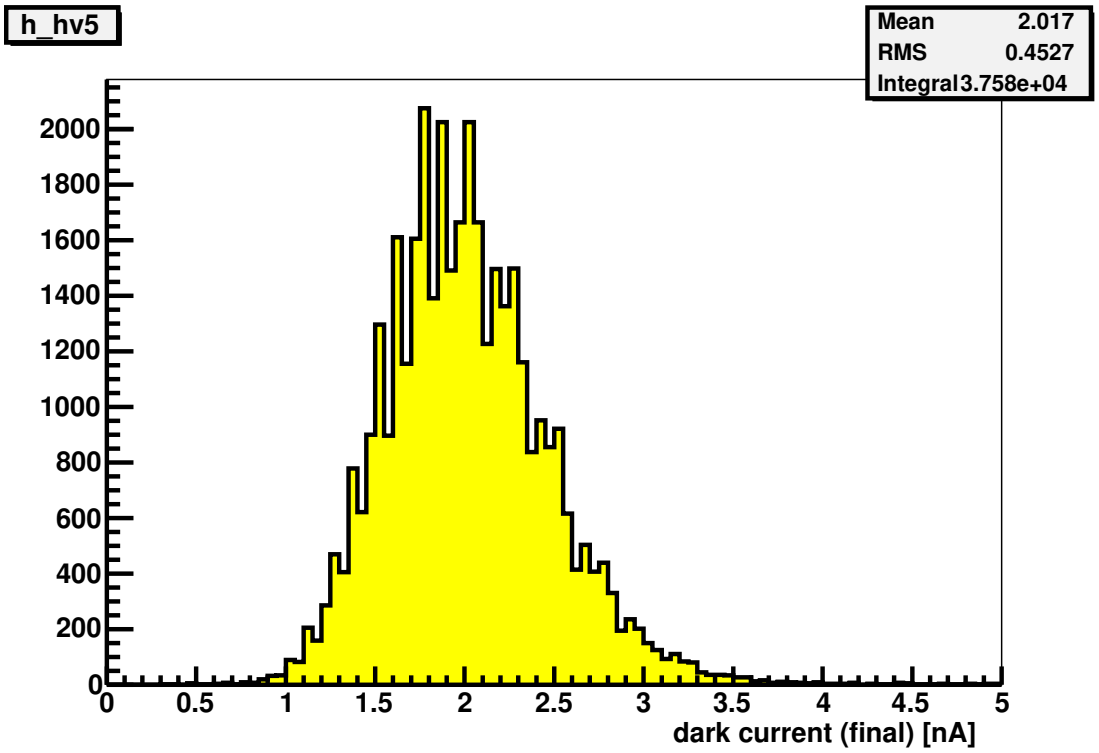

Figure 9: *a: Dark current in nA of all used tubes.*

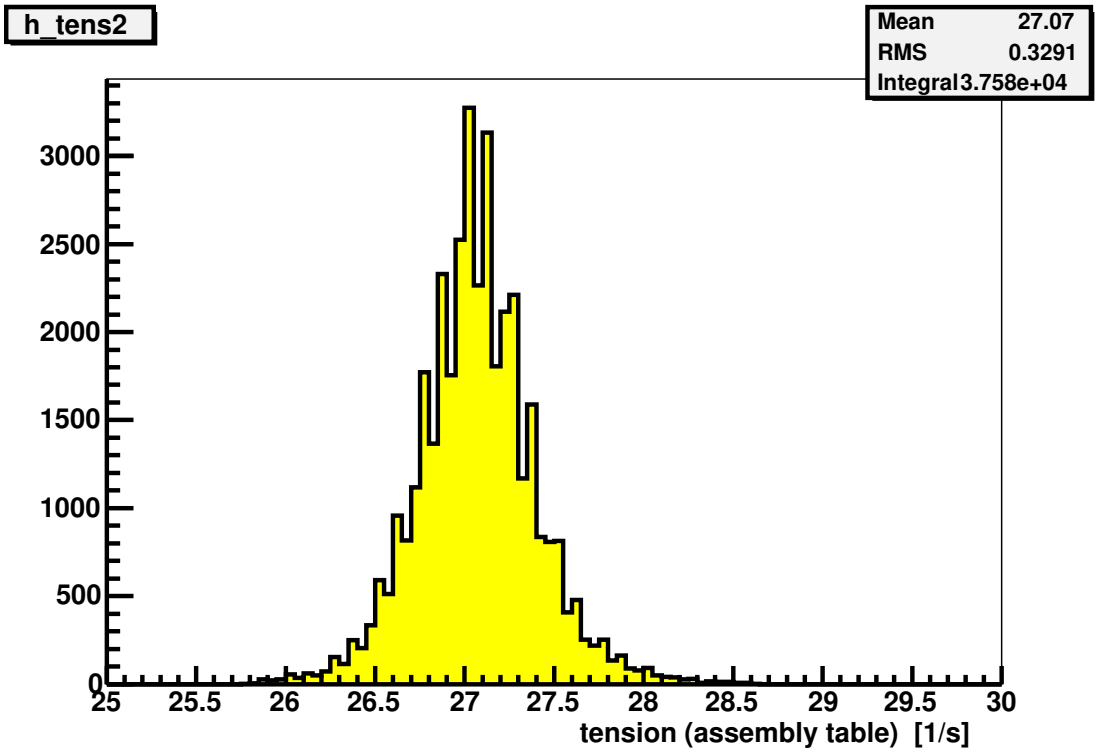

Figure 10: *Measurement of the wire tension of all tubes just before chamber assembly.*

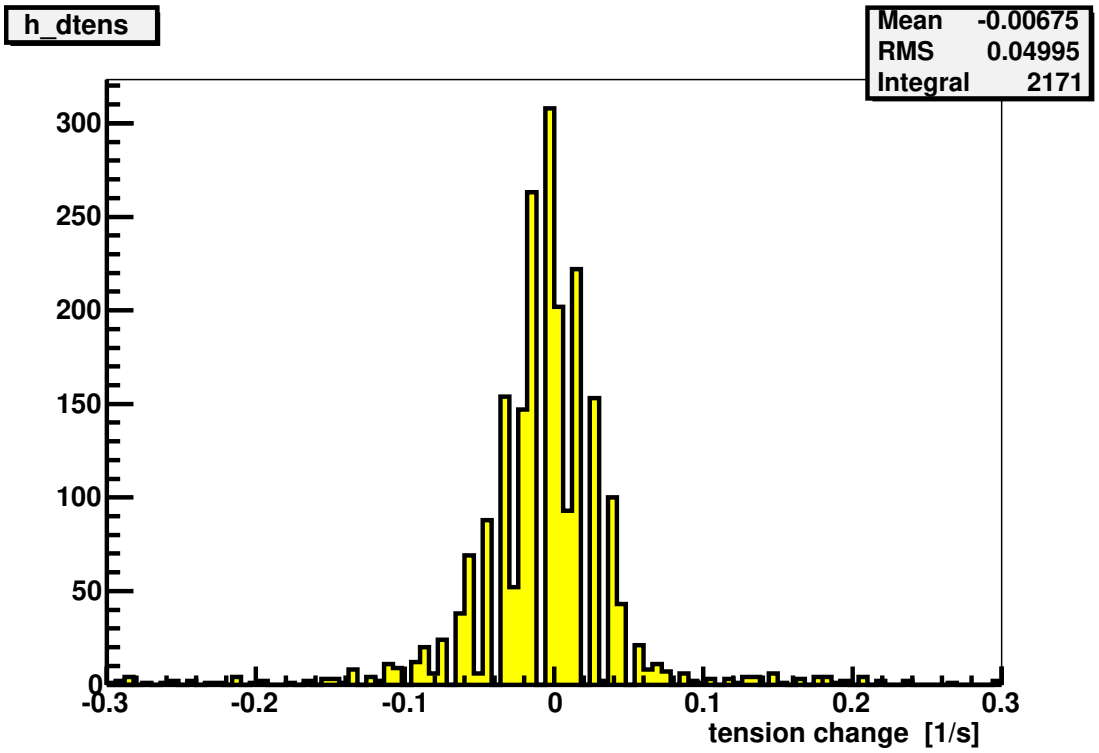

Figure 11: *Measurement of the change in wire tension between production of the tube and chamber assembly.*

4 Drift tube chambers

Above we already showed in figure 3 the mechanical layout of a BOL chamber. The aimed mechanical precision of 20 μm RMS is implemented as follows. Any transverse cross section of any chamber can be represented by a single wire grid. The individual wires of a particular chamber are mapped on this grid with residuals distributed within 20 μm RMS. Note that this precision applies to the wires, while the tubes have a looser position requirement of 100 μm RMS (with respect to the wire).

The BOL chambers have a length of 5 m and come in three different widths: 2160 mm (72 tubes/layer), 1680 mm (56 tubes/layer) and 1440 mm (48 tubes/layer), all with two multilayers with 3 tube layers on each side of the spacer.

The spacer is constructed of three 'I' beams, called cross-plates, running orthogonal to the tubes. The cross-plates have low mechanical precision (0.5 mm) and the glue (3M xxxxxxxxx), which connects to the mulilayers, absorbs possible irregularities. The crossplates are connected by two beams, that run longitudinal (which are therefore called long-beams). The horizontal position of the central cross-plate with respect to the long-beams is adjustable to compensate for gravitaional sag of the chamber. A schematic view of the sag adjustment system is shown in figure 12.

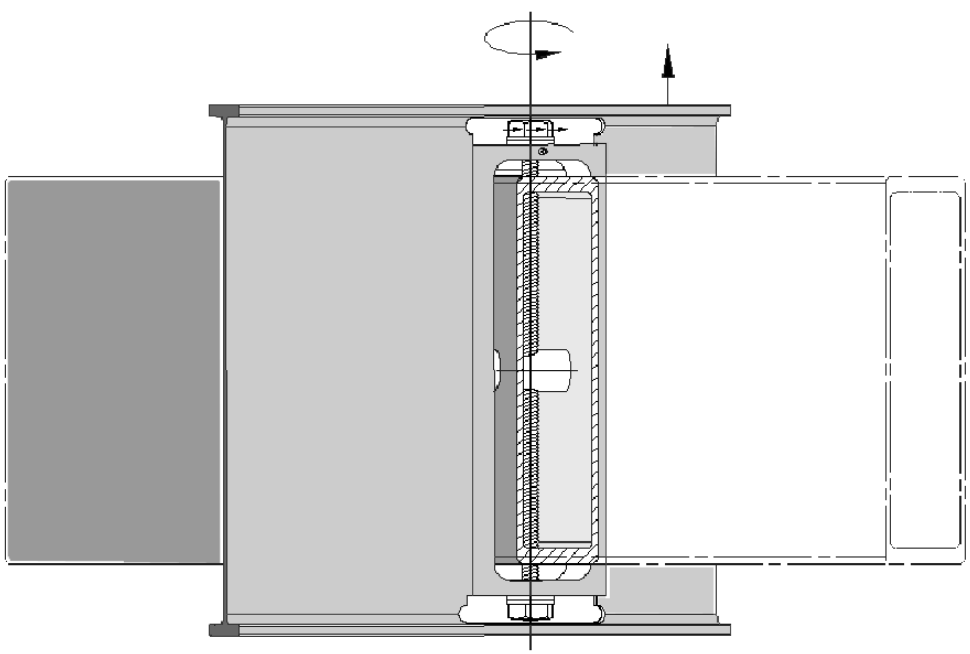

Figure 12: *Schematic view of the sagadjustment system in the middle crossplate. Shown is the longbeam that is connected to this crossplate with a SPINDEL. By simply turning the SPINDEL the heigth of the middel cross plate with respect to the longbeam and is adjusted, enabling to align the middle crossplate with respect to the outer crossplates.*

For the in-plane alignment system, two camera's and four masks are mounted on the RO and HV crossplate respectively and the central crossplate houses four lenses. With two parallel and two diagonal light rays several deformations of the spacer and thus chamber can be monitored; most notably the sag and torque of the chamber. The torque is a relative rotation of the two outer cross-plates. A total of 10 temperature sensors are mounted on the crossplates to monitor temperature gradients.

Tubes of the same layer lie in the same plane. The tubes of an adjacent layer is shifted by 15 mm (the half of the tube's width) and stacked as illustrated in figure 13.

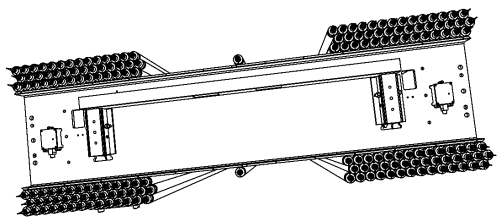

Figure 13: *Schematic view of a chamber with several tubes left out to illustrate the stacking of tubes into layers.*

Tubes of the same layer are grouped in series of three (tripplets) to reduce the number of gas connections to the on-chamber manifold. Only the first and last tube in the tripplet connects to the manifold at the RO side and HV side respectively, while the tubes are connected with plasticxxxxx gas jumpers. The mounting of electronic boards, equipped with xxxxconnections, is carefully prepared by fixing the rotation of the tubes such that the ground pins finally lie in line within 0.5 mm. In the next chapter we elaborate on the on-chamber services.

Practically, the position requiment of 20 μm on the wires implies that the drift tubes should be accurately assembled into a chamber near the endplugs at the outer cross-plates. The straihgtness of the tubes in between the endplug is of less importance. Therefore, we aimed to set-up an assembly stand based on a granite table with precision mechanics, such as jigs to hold the drift tubes, machined with a precision of 10 μm or better. During assembly, the position of the spacer and individual tubes near the outer cross-plates need to be monitored to the same level.

4.1 Assembly station

The gluing of six layers of 72 tubes onto a structure with dimensions 5m $\times$ 2m , with a precision of 20 μm is a delicate procedure. Depending on the actual layer to be glued, mistakes are costly in time and material. We constructed an accurate assembly station and adopted a robust procedure to assemble the muon chambers with high precision. A picture of a mecanically completed BOL chamber on the assembly station is shown in figure 14. Below, we describe in detail the setup and the assembly steps.

Figure 14: *finished BOL*

Figure 15 shows the granite table equipped with precision mechanics. The cartesian coordinate system and the north (N), south (S) and west (W) sides are also indicated. All jigs are equipped with vacuum suckers to hold the tubes firmly positioned. The end-plugs are hold by the outer jigs, which are constructed and positioned with a tolerance of 10 μm . The jigs are fixed at the west side, the reference side, and can expand freely to absorb temperature variations. These components, combined with a stable and uniform temperature (typical variation $< 0.5°$C over one day) allow to assemble chambers within the 20 μm RMS precision requirement.

During assembly, extensions with precise spheres (diameter 6cmxxxx) are mounted on the cross-plates as can be seen in figure 16a. These extension house a RASNIK-mask, monitored by the so called RASNIK monitoring system as indicated in the figure. Using exchangable blocks (also indicated in the figure), the stacking towers have adaptable heights to absorb the thickness of the vertical pitch of the tube layers. The central stacking position is shifted by half the horizontal pitch as appropriate. The stacking towers at the reference side support the spheres with so-called sphere-holders that can move freely in the x direction to absorb temperature variations. At the east side, the non-reference side, the sphere-holders can move freely in the horizontal plane. The sphere-holders are designed such that their height during possible horizontal movements is maintained with an accuracy better than a few microns.

When the spacer (with or without already fixed tube layers) is supported by the stacking towers the gravitational of the cross plates is considerably, of the order of 50 μm . To reduce this sag considerably to typically 10 μm the unfinished chamber is carried by an additional system. One of the the eight pneumatic cylinders constituting this system is also visible in figure 16b.

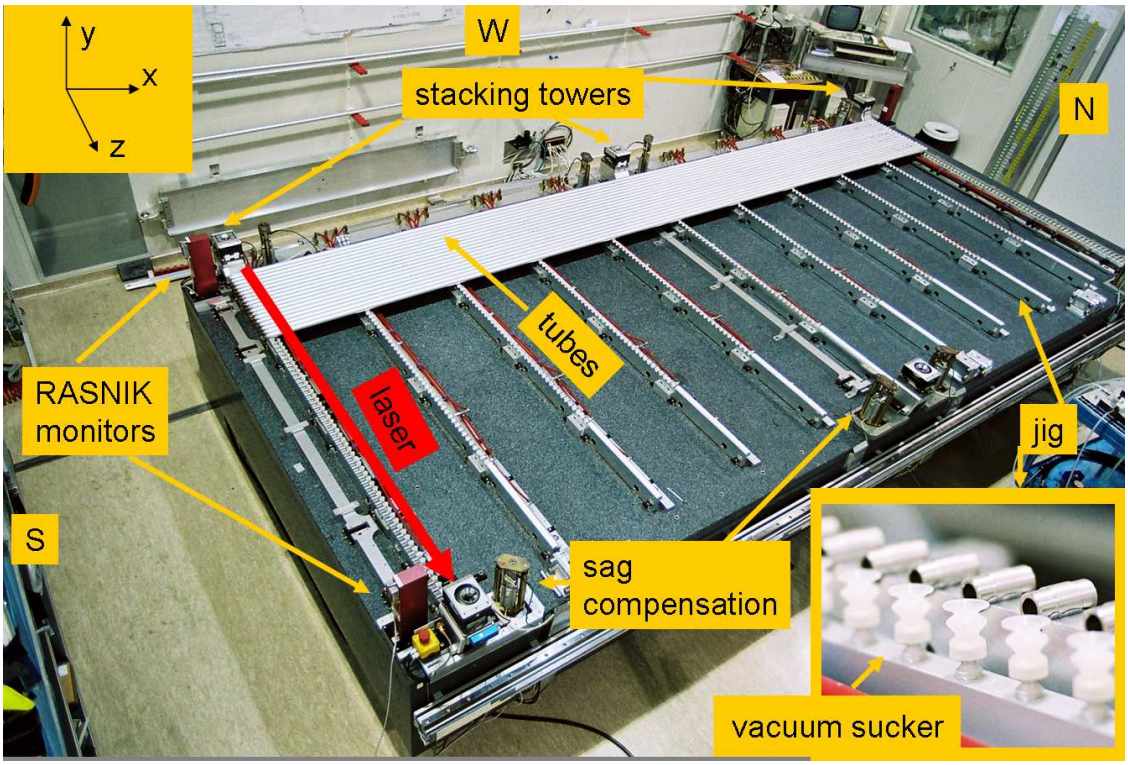

Figure 15: *Picture taken in the cleanroom showing the assembly table. Several key items are indicated.*

After the construction of every 25-th chamber several checks concerning the accurate positioning of the mechanics were performed. Notably, the distances between the corner stacking towers and the corresponding jig at the RO and HV reference side was measured with an auxiliary device. When these distance deviate, the chamber obtains an unwanted stereo angle build in. Our checks demonstrated that such stereo angle is smaller than 4 μrad over the full period of the production.

4.2 Chamber assembly

The assembly procedure starts outside the cleanroom with the construction of the bare spacer, with a 'loose' accuracy of typically 500 μm . Then, in the cleanroom, the tubes are attached layer by layer using glue. This process typically takes half a working day, but the time needed for the glue to cure, constraints the production-speed to one layer a day.

As already mentioned the quality control during chamber assembly start with re-measuring the wire tension of the tubes to be glued in the particular sequence. After this test, the tubes are positioned in the jigs and the gas jumpers are temporary fixed in a way such that tube length differences within a triplet are absorbed as illustrated in in figure 17, which ensures a tight connection of the jumpers on the tube. Additionally, to position the end-caps of an entire tube layer in-line, we use jumpers of appropriate thickness (in steps of 100 μm , maximal 300 μm), which later on facilitates the the mounting of electronic boards.

After this procedure, the jumpers are loosened to avoid unwanted stress between neighboring tubes that could prevent the tubes to fall into their jig position. Then, position of the end-plugs, both at the RO and HV side, is measured using laser beam running parallel to the end-plugs [7] as indicted in figure 15. For this test, a reference rod is placed between two adjacent tubes which partially blocks the laser beam measured by an optical sensor. Deviations in the response respresent a measure of deviations in tube heigts. Note that by measuring between adjacent tubes, the results of this test are somewhat ambiguous in case neighbouring tubes are both badly poistioned. In addition, the test is sensitive to tube heights (y) as well as to the distance (z) between tube pairs and the radii of the corresponding end-plugs. On the other hand,

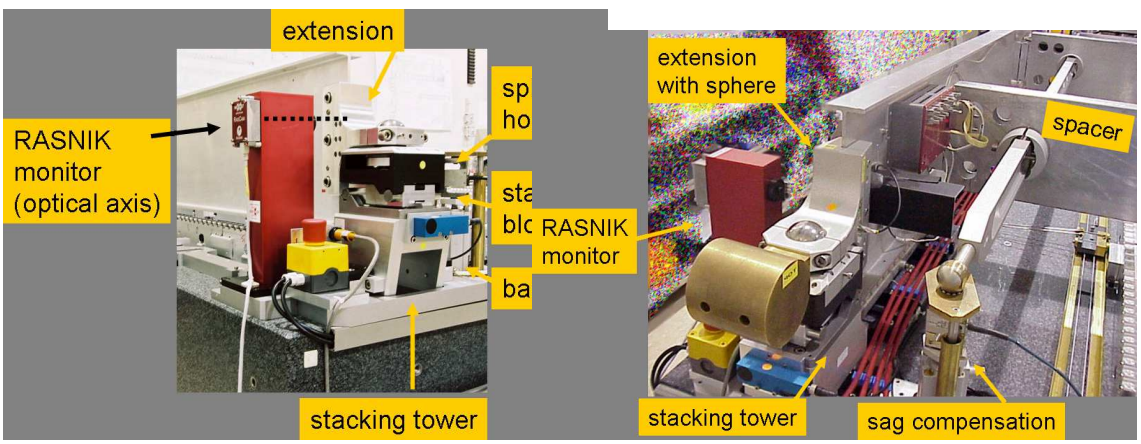

Figure 16: *a) The picture shows the stacking tower supporting the sphere in the extension of the spacer. The position of the extension is monitored by a RASNIK alignment system. b) This pictures shows the stacking tower together with the sag compensation tower.*

a badly positioned tube shows up twice and is tagged easily. In practice, only a few tubes needed to get re-positioned. In some rare cases, we had to replace the complete tube due to, as it turned out, bad swaging of the end-plug. Bad swaging occurred for a particular batch of tubes where the end-plug was not well inserted in the aluminium tube. We aimed at tube height deviations below 20 μm and investigated all tube pairs with responses above 10 μm were inspected by the operators. The result of these measurements as shown in figure 18, indicate that the tubes are well positioned.

After position of the tubes glue (Araldytexxxxx) is dispensed by means of an automated gluing machine as shown in picture 19a.

For the first (and later second layer), glue is dispensed only in between adjacent tubes. The relevant side of the cross-plates is supplied with a sufficient amount of glue (3Mxxxxxx) and the spacer is lowered onto the tube layer. The correct positioning of the spacer is checked using the RASNIK systems that monitor the cross-plate extensions at the four stacking towers at the corners of the assembly table. In addition, we used a temporary RASNIK system on both the HV and RO crossplate to monitor their sag. Together with the 'standard' in-plane alignment components of the spacer, these RASNIK systems provided crucial position information with an precision of 10 μm , which may be regarded as remarkably accurate for such large structure.

PLOTRASNIK, Graziano

After glue curing for at least 12 hours the spacer with the first tube layer is rotated upside down, effectively over its x axis, thus respecting the reference side. The second tube layer is prepared the similar procedure as for the first layer is followed. Now both sides of the spacer have a tube layer attached to it. To glue the third layer, the spacer is lifted and the stacking tower height is adapted to attach the third tube layer. On the tubes of the third layer and onward, two additional glue ropes (Araldytexxxxx) are dispensed to connect adjacent tube layers. To glue the fourth layer, the spacer with its three tube layers is rotated back to its original orientation, limiting the (un)balance of the spacer and tube layers and thus avoids possible

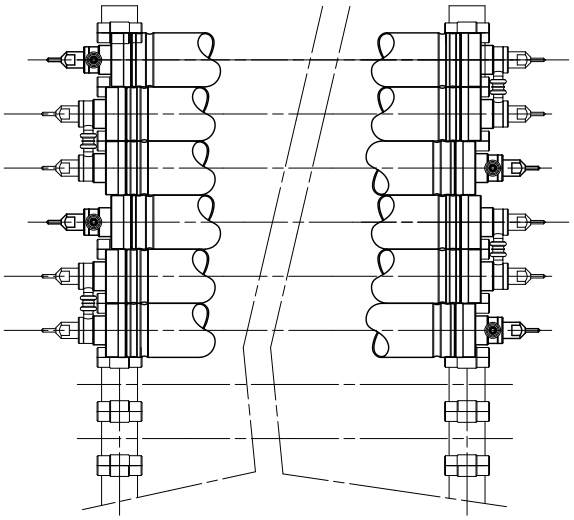

Figure 17: *Illustration of gastriplets.*

effects of asymmetrical weight distribution. After gluing the fifth layer, one multilayer with three tube layers is finished.Figure 20 shows the distribution of glues between the tubes in a finished multilayer. The chamber is turned once more to finish it by attaching the sixth layer. A picture of the final chamber still on the granite table was already shown in figurebolaf.

4.2.1 Results of X-ray scans

About 10% of all chambers undergo a mechnical precision check in X-ray tomograph [6] at CERN. The tomograph consists of a unit with two stereo X-ray beams that runs over the chamber in the z direction at a fixed x position. Scintillator counters measure the 'shadow-pattern' of the wires and tube-walls. A dedicated analysis of such pattern results in a wire position map with an accuracy of typical 5 μm . The chamber is considered certified as the distribution of the residuals with respect to the nominal wire map has an RMS below 20 μm . Table 1 lists the RMS values of the residual distribution for the scanned BOL chambers. The numbers indicate that these chamber are assembled according to the specifications.

	RMS z μm	RMS y μm	RMS combined
BOL 2	1000	0000	0
BOL 3	1000	0000	0

Table 1: *The table list for each scanned BOL chamber the residuals of the wire coordiantes obtained in the X-ray tomograph. The numbers of the BOL chambers refer to their serial production number.*

In figure. 21 we compare the layer Z-pitch deviations obtained by the X-ray tomograph with those derived from the RASNIK monitoring at the time the layers were glued. The RASNIK deviations are shifted to set their average deviation to zero as appropriate for this comparison. The distribution of the differences of the two measurements has an RMS of 6 μm , indicating that the quality control during the assembly is

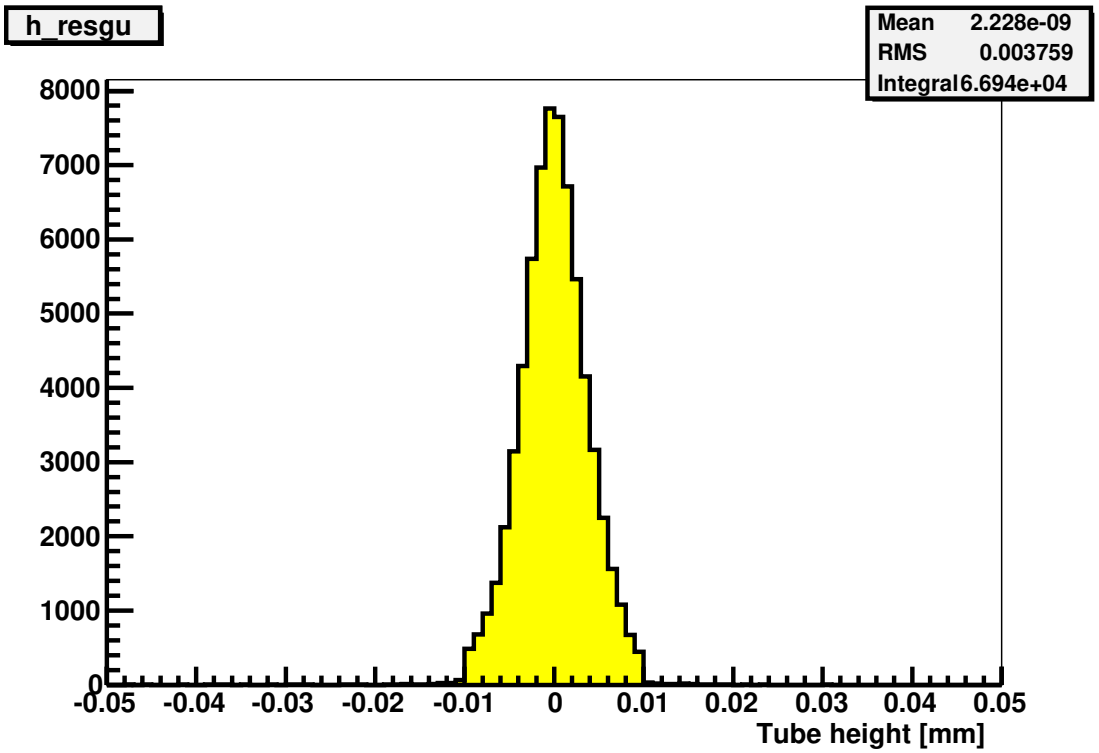

Figure 18: *Tube positions during assembly.*

well understood.

Figure 19: *a) Glue dispension by the gluing machine. b) attaching another layer.*

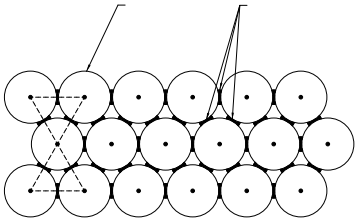

Figure 20: *Illustration of the distribution of glue between the tubes in a multilayer.*

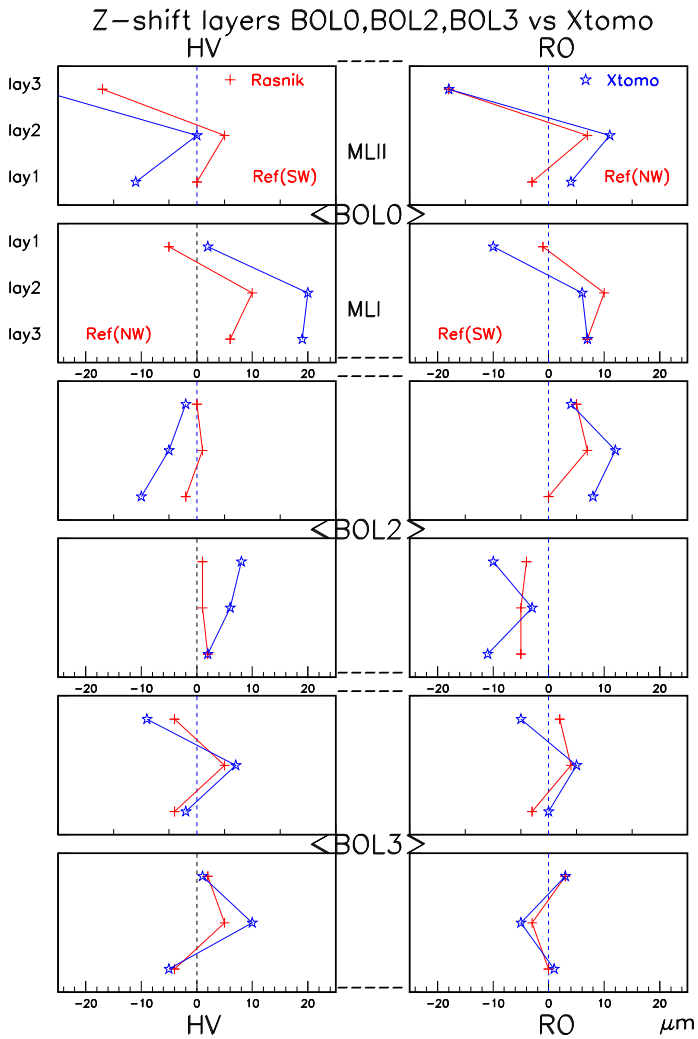

Figure 21: *Comparison of results from the tomograph scans for chambers BOL0, BOL2 and BOL3 with RASAS data taken during glueing of the layers of these chambers. For each chamber a set of 4 plots show the deviations from the nominal Z layer pitch for the 3 layers within each multilayer (MLI and MLII) at the HV and RO side respectively. xxxxxxxxxxxxxxxxxxkeep it? Then, renew itxxxxxxxxxxxxxxxxx*

5 Chamber services

Alignment components As mentioned before, physical deformations of the chambers are monitored with the in-plane alignment system consisting of four RASNIK systems mounted during chamber construction. The inter-chamber alignment consist of RASNIK systems monitoring the position of neighbouring chambers of the same type and RASNIK systems that monitor the projective alignment of the three muon chamber layers. In a test setup at CERN [2] it was demonstrated that this system achieves an alignment accuracy better than 10 μm (on the change of the relative chamber positions). After chamber construction the mounting platform for these system are glued on the chambers. The components for the in-plane RASNIK systems are shown in figure 22. The power and readout for all alignments systems is provided by an on-chamber multiplexer, called RASMUX, which itself is later connected through one D-25 cable to a master system that steers and collects information of several muon chambers. The RASMUX is also shown in figure 22.

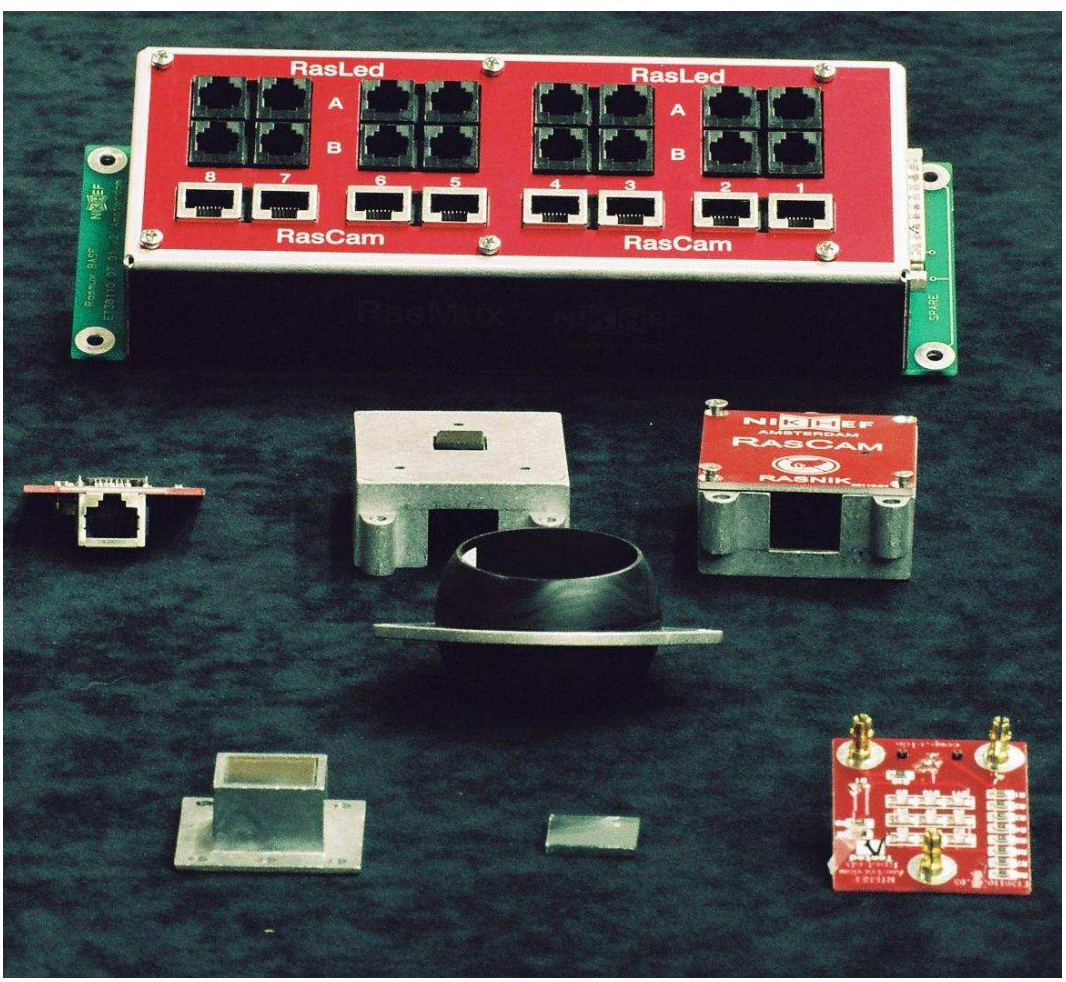

Figure 22: *Picture of several alignment components.*

Temeprature and magnetic field sensors A total of 18 temperature sensors provide supplementary information on possible chamber deformations. In addition, typical a few magnetic field sensors probe the field for off-line corrections. These sensors connect to the detector control system (DCS). The DCS is configured and readout with the CAN protocol.

Gas system The on-chamber gas system consists of two gas manifolds for each multilayer. Tubes of

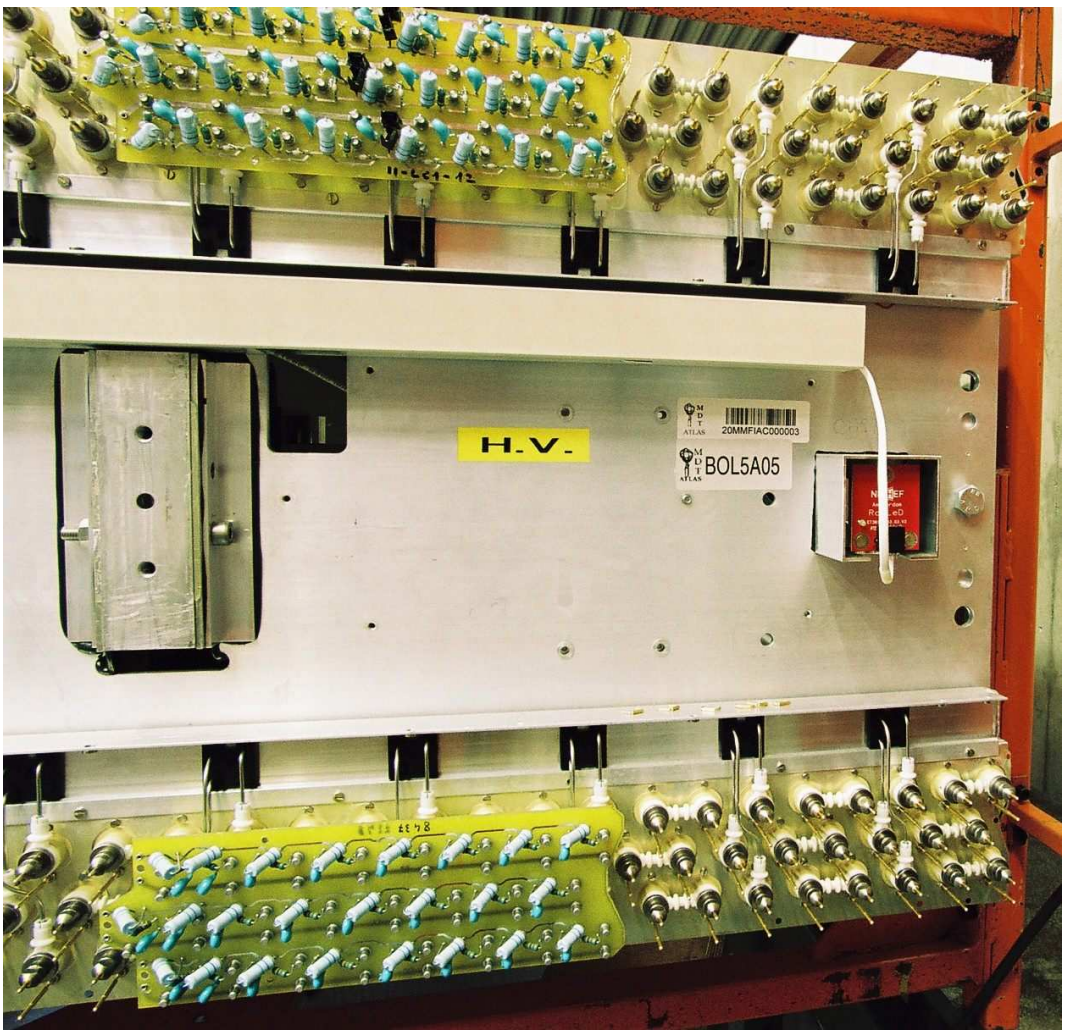

Figure 23: *Picture taken the HV side of a BOL chamber. Some individual tubes can be recognized together with the connections to the gasmanifolds. Also shown is a HV board and the backplate of the RASNIK mask component.*

the same layer are grouped in series of three (tripplets) to reduce the number of gas connections to the manifold. Only the first and last tube in the tripplet connects to the manifold at the RO side and HV side respectively. After installing the gas system, the chamber is filled to 3 bar and its pressure (corrected for temperature effects) is monitored for at least 24 hours to assure the gas tightness of the added components. The manifolds have only one input or output and can be quickly connected to the gas service in the experiment.

Electronics All the tubes in the chamber are provided with a ground pin at the RO and HV side respectively. The ends of the ground pins and the pins on the gas caps all lie in the same plane as can be seen in figure 23. The and HV electronic boards are provided with xxxxxxxxxxconnetor to connect to the pins robustly. The digital signal processing and the final time measurement is embedded on so called 'mezzanine' cards that directly connect to the analogue RO electronics and are housed in individual faraday cages. The digitized signals are shipped to a central on chamber processor card (CSM) as shown in figure 24. The CSM is configured via the DCS and connects to the experiment data acquisistion system by optical fibers.

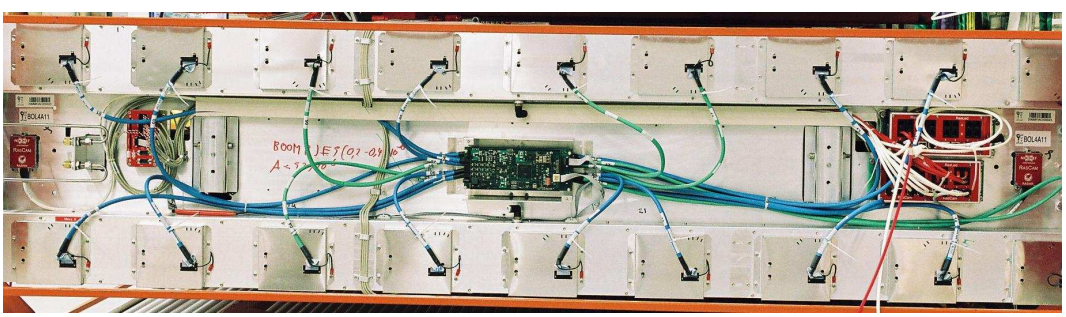

Figure 24: *Picture taken at the RO side of a nearly completed BOL chamber. The RO electronics of the top and bottom multilayer is enclosed in Faraday cages. Also visible are the backplates of the RASNIK cameras, the DCS control box for the temperature and B field sensors, the readout motherboard and two RASMUXes as required for this specific chamber.*

6 Broken wires

WHERE??????????????????????????? After the completion of the first chambers we detected a number of broken wires in several chambers. Despite many dedicated studies, the cause of this problem has not been recovered. However, we observed that broken wires seem to occur only in chambers that have 'seen' high gas flows (xxxbar/l). Moreover, this problem is restricted to the first (or last) tube of a triplet connecting to the gas manifold. To avoid such high flows we put mechnical flow restrictors in the on chamber gas outlet tubing. In total we have xxxx chambers with broken wires. Usually, the number of broken wires is limited to 1xxxxx, except for one chamber, BOLxxxx, whch has the 24xxxx broken wires. We repair the broken wires, using a procedure that uses the existing o-ring and thus not requires any glue. This comes not for free. The accuracy of the wire position is estimated to a few 100 μm . In principle, the wire position of such wires can be obtained later in the ATLAS experiment with a procedure that uses tracks xxxxxxxxxxxxxxxxmore?.

7 Tests of completed chambers

The main purpose of the test stand is to verify the electronic read-out of each chamber under ATLAS gas (Ar/CO_2= 93%/7% at 3 bar) and HV (3300V) conditions.

7.1 Cosmic ray test stand

The cosmic ray test facility at NIKHEF accomodates five BOL chambers and has a fixed trigger system as shown in figure 25. The trigger units (also visible in the figure) consist of two layers of scintillators, separated by 50cm thick iron block to filter out the low energetic muons (i.c. muon with energies smaller below 0.7 GeV). Since the summer of 2004 till the autum of 2005 we routinely tested BOL chambers; usually we exhanged three chamber middle chamber and kept the outer chamber in place to have a stable reference.

Figure 25: *Picture of the cosmic ray stand with five BOL chambers. The chamber in the in the highest position is a small type BOL chamber with a width of 48 tubes.*

7.2 Results

Figure 26 show a typical difttime distribution for a single wire. The t_0 and t_{max} for each individual wire is extracted from its drifttime distributions. Large deviations are a good indicator for problems. We often observed a pattern related to groups of three drift tubes constituting a gas-tripplet. After an extended period of flushing (xxxxxxx liter) these structures disappear. One, and only one, severe problem remains, which are the broken wires observed in some chambers as mentioned above. xxxxxxxxxx

Further analysis of the data uses software being developped for ATLAS and involves driftdistance versus drifttime calibration with corresponding track fits to drift circles in individual chambers. The distribution of the residuals for a representative wire is shown in figure 27.

DUMMY FIGURE

Figure 26: *Drift time distribution xxxxxxxxxxxxxget xxxxxxxxxxxxxxxxx*

DUMMY FIGURE

Figure 27: *Residual. xxxxxxxxxxxxxget plot if we want it.xxxxxxxxxxxxxxxx*

The efficiency for single hits is 9xxxx% and the resolution is xxxxxx μm as expected for the current conditions.

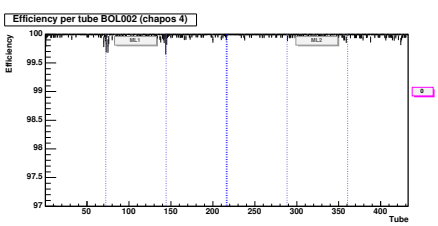

Figure 28: *Efficiency for BOL002 as a function of the tube number.*

ONDERWERPEN/FIGUREN:

- hit distributions
- drift properties: TMAX
- efficiencies
- tracks
- problems
- wire/layer locations (correlations XTOMO)

8 Chamber transport to CERN and instalation in ATLAS

ONDERWERPEN:

handling tools, common supports, RCP assembly

Figures:

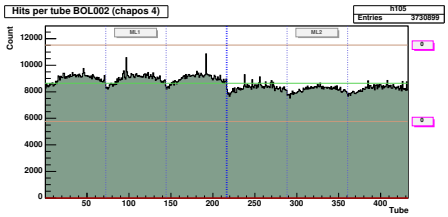

Figure 29: *Hit distribution for BOL002 as a function of the tube number.*

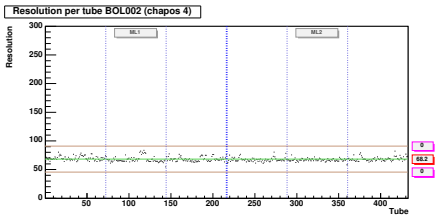

Figure 30: *Resolution for BOL002 as a function of the tube number.*

- Trasnport frames
- Work at CERN: common support
- BOL above magnet (photo exists already)
- installed BOLs

9 Conclusions

chambers are within specs.

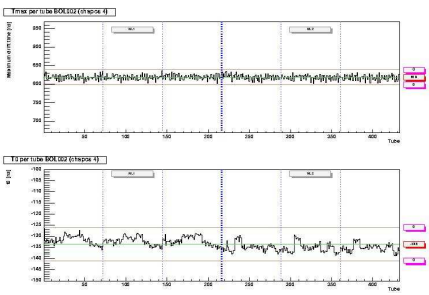

Figure 31: *The t_0 and t_{max} distributions for BOL002 as a function of the tube number.*

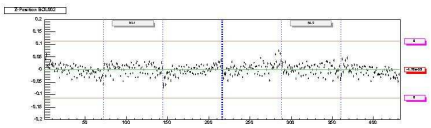

Figure 32: *Wire position deviation in the z direction for BOL002 as a function of the tube number.*

References

[1] The ATLAS MUON TDR, http://atlasinfo.cern.ch/Atlas/GROUPS/MUON/TDR/Web/TDR.html

[2] First System Performance Experience with the ATLAS High Precision Muon Drift Tube Chambers Poster presented by M. Vreeswijk at Vienna WCC 1998. Published in Nucl.Instrum.Meth.A419:336-341,1998
http:atlasinfo.cern.chAtlasGROUPSMUONdatchadatcha.html

[3] M. Woudstra, PhD Thesis, to be published

[4] ELECTROSTATIC DIGITAL METHOD OF WIRE TENSION MEASUREMENT FOR KLOE DRIFT CHAMBER. A. Andryakov et al.. 1998. Prepared for 7th Pisa Meeting on Advanced Detectors: Frontier Detectors for Frontier Physics, La Biodola, Isola d'Elba, Italy, 25-31 May 1997. Published in Nucl.Instrum.Meth.A409:63-64,1998
MDT wire tension measurement using an electrostatic method, ATLAS internal note, ATL-MUON-38-264.

[5] An electromagnetic micrometer to measure wire location inside an ATLAS MDT drift tube, Cambiaghi, M., Cardini, A., Ferrari, R., Gaudio, G., ATLAS Internal Note ATL-MUON-1998-259, 1998

[6] tomograph

. M. Cambiaghi et al., Proceedings of the 1999 IEEE Nuclear Science Symposium, IEEE Trans. Nucl. Sci. 47 (3) 2000.

[7] ATLAS Internal Note MUON-NO- 29 September 1998 A QA/QC system to monitor the planarity of the tube layers in MDT chambers construction G. Ciapetti, G. De Zorzi, R. Giacalone, L. Montani, D. Pinci Dipartimento di Fisica, Universit di Roma "La Sapienza" and INFN, Sezione di Roma

[8]

[9] C. Bini *et al.*, Nucl. Instrum. Meth. A **461** (2001) 65.

[10] The RASNIK alignment system. To be published in Nucl. Instr. and Meth.

A Alignment system RASNIK

The Red Alignment System NIKhef (RASNIK) consists of a coded mask, a lens and a video image sensor [10]. The mask, illuminated with (infra-red) LEDs from behind, is projected by the lens onto the image sensor as illustrated in figure 33. A daylight-blocking filter is placed before the image sensor. If the lens is displaced in the direction perpendicular to the optical axis, then the image on the sensor will be displaced in the same direction, magnified with a factor $(v + b)/v$, where v is the object distance and b the image distance. If the lens is displaced along the axis, the image scale S will change following $S = b/v$. Finally, if the mask rotates around the optical axis with respect to the sensor, the image rotates accordingly. From the analysis of a RASNIK image, four parameters can be deduced: two tranversal displacements, one displacement along the optical axis, and the relative rotation between the mask and sensor around the optical axis. The changes are relative: a common shift of three components does not change the readout values. The changes can be expressed, for instance, in terms of a mask displacent or a lens displacement.

A typical RASNIK image is shown in figure 34, clearly displaying the chessboard pattern, in which each 9th row and 9th column is carrying a digital code. This code has the values (0,0) in the bottom left of the masks, and increases linearely with the coded column and row numbers into the direction of the top-right corner in the mask. In this way the coarse position of the image, showing only a small part of a large mask, can be identified.

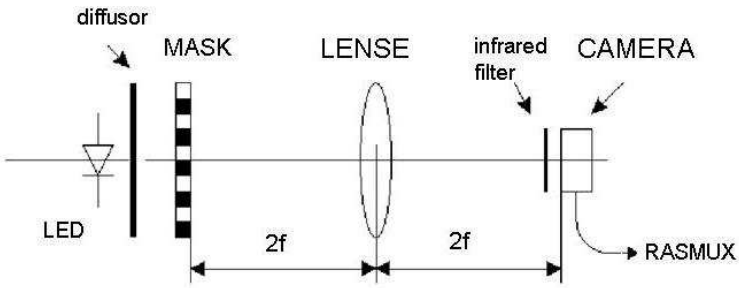

Figure 33: *The principle of RASNIK.*

The video signal of the sensor is digitised by means of a frame grabber in a pc. After differentiating the image data, the contours of the chess fields appear as an orthonormal grid pattern. From this, the 'fine' image position, image scale and image rotation are obtained. After detecting and decoding the 9th row and columns, the coarse image position is obtained.

Due to the large summed length of chess field contour on an image (100 mm, in both directions), a precision of 50 nm (RMS) is obtained in the two transversal directions in terms of image position on the sensor, per image. The image scale is measured with a resolution better than 5×10^{-5} (RMS), and the resolution of the image rotation is 20 μrad (RMS). When placed in air, the RASNIK performance is limited by the gradients and fluctuations in the gradient of the air temperature. The linearity of the system is exclusively determined by the precision of the mask. For ATLAS, we applied low- cost 'contact copies' of mother-masks made in VRSI industry, and their precision was guarantied to be better than 0.1 μm . The range of a RASNIK system is determined only by the mask size, and can be as large as 125 $\times$ 125 mm^2. For the InPlane systems we applied mask segments of 20 $\times$ 20 mm^2, and for the projective systems masks of 50 $\times$ 50 mm^2 were used.

A RASNIK system can be calibrated by placing the three components in a well known relative position, while recording the readout values. After that, the deviation from the initial alignment can be obtained from the difference between the actual readout values and the calibration values.

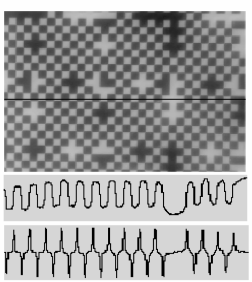

Figure 34: *Typical RASNIK image with the chess sboard pattern and the coded row and columns. The light intensity of the pixels under the indicated line is plotted, together with its derivative. The Gaussian peaks (positive and negative) determine the fine position of the image, as well as the image scale.*